Chinese Chemical Letters 31 (2020) 3195–3199

Contents lists available at ScienceDirect

Chinese Chemical Letters

journal homepage: www.elsevier.com/locate/cclet

Communication

Self-assembled fluorescent tripeptide nanoparticles for bioimaging and drug delivery applications

Dongjie Fu, Dingchang Liu, Lianbing Zhang, Leming Sun*

School of Life Sciences, Key Laboratory of Space Bioscience & Biotechnology, Northwestern Polytechnical University, Xi'an 710072, China

ARTICLE INFO

Article history:
Received 29 May 2020
Received in revised form 6 July 2020
Accepted 6 July 2020
Available online 7 July 2020

Keywords:
Self-assembly
Tripeptide
Fluorescent nanoparticles
Bioimaging
Doxorubicin
Drug delivery

ABSTRACT

Peptide self-assembled nanomaterials have attracted more and more attention due to their wide applications such as drug delivery, cell imaging, and real-time drug monitoring. However, the application of the peptide is still limited by its inherent optical properties. Here we proposed and prepared a series of fluorescent tripeptide nanoparticles (TPNPs) through π-π stacking and zinc coordination. The experimental results show that the nanoparticles (TPNPs1) formed by the self-assembly of the tripeptide tryptophan-tryptophan-tryptophan have the highest fluorescence intensity, uniform and appropriate size, and low cytotoxicity. Furthermore, there was fluorescence resonance between TPNPs1 and doxorubicin, which has been successfully applied for real-time cell imaging and drug release monitoring.

Over the past decade, nanoparticle-based delivery systems have been extensively explored in biomedical fields for the prevention, diagnosis, and treatment of diseases [1–4]. The nanoparticle systems have unique properties that can increase drug solubility, enhance drug targeting, modulate release profile, load, and deliver multiple drugs simultaneously [5–8]. Compared with the use of inorganic nanoparticles for drug delivery, the low toxicity and easy degradation of peptide nanoparticles give them a greater advantage in biomedical applications [9–12]. On this basis, peptide nanoparticles with fluorescent properties are widely used for bioimaging and nanocarriers due to their unique optical properties, but the inherent optical properties of peptides limit further applications [13–16]. It has been proposed to use quantum dots to modify polypeptides to change their optical properties, but the high cytotoxicity limits their application [17–19]. Although organic fluorescent dyes could be used to modify polypeptides, the high specificity makes the limitation of their applications [20]. Fortunately, by regulating the self-assembly process, the optical properties and morphology of the nanoparticles formed by peptides can be changed. Therefore, it is very important to synthesize peptide nanoparticles with new optical properties by regulating the self-assembly environment.

Previously, it has been reported that zinc-coordinated fluorescent dipeptide nanoparticles can be used as functional nanoprobes for targeted cancer cell imaging and real-time monitoring of drug release [14]. Moreover, cyclic peptide self-assembled fluorescent nanoparticles also have been demonstrated for the treatment of esophageal cancer [15]. According to previous reports, it was known that by initiating the interaction between ions and peptides, zinc ions could be pulled into a peptide-rich low-dielectric environment to form a more complex ordered structure, which can enhance fluorescence and promote peptide self-assembly [21]. The π-π stacking between benzene rings of chiral amino acids also can provide a driving force for peptide self-assembly [22–24]. Similarly, the green fluorescent protein (GFP) in nature has a π-π stacking phenomenon due to the mutation of threonine at position 203 to tyrosine, which in turn causes the fluorescence to shift to the red spectrum to obtain yellow fluorescent protein (YFP) [25]. It is also the mutant with the longest emission wavelength among all GFP mutants. Therefore, π-π stacking can be used to regulate the fluorescence properties of peptide nanoparticles while promoting the self-assembly. Moreover, BFPms1, one of the GFP mutants, could enhance the fluorescence due to its high affinity with zinc ions. Therefore, the fluorescence can be enhanced by zinc ions.

Inspired by the above mechanisms, we proposed to use the metal ion coordination and the π-π stacking effect to regulate the fluorescence properties of the peptide assembly and explore its role in drug delivery and cell imaging. On this basis, we first selected linear tripeptide as the self-assembly unit to prepare tripeptide nanoparticles (TPNPs). The results showed that under ultraviolet light, TPNPs can stimulate fluorescence in the visible

* Corresponding author.
E-mail address: lmsun@nwpu.edu.cn (L. Sun).

https://doi.org/10.1016/j.cclet.2020.07.011

region. Moreover, the emission region of TPNPs overlaps with the excitation region of doxorubicin (DOX), indicating that TPNPs can be utilized as a fluorescent probe to monitor DOX release in real time. The complex formed by TPNPs and DOX can release DOX in low concentration environment, the results also demonstrated that TPNPs could be used as a nano-platform for cancer cell imaging and drug delivery applications.

Detailed experimental procedures are shown in Supporting information. In this experiment, fluorescence properties of self-assembled peptide nanoparticles were regulated by using the π-π stacking interaction and metal ion coordination effect under the appropriate pH environment. Among the three aromatic amino acids, tryptophan has the highest number of π electrons, which can provide delocalized electrons for fluorescence. At the same time, the π-π stacking between tryptophan benzene rings can be used as the self-assembly driving force while promoting the change of optical properties. Therefore, three kinds of tripeptides containing natural aromatic amino acids and one candidate containing no aromatic amino acids for the experiment were selected: WWW (Trp-Trp-Trp), WWE (Trp-Trp-Glu), WEW (Trp-Glu-Trp), and EEE (Glu-Glu-Glu) respectively. To illustrate the molecular weight of the peptide and understand the four tripeptides more intuitively, mass spectrograms of the four tripeptides were obtained (Figs. S1–S4 in Supporting information).

A series of experiments were carried out to investigate the relationship between the self-assembly process and the optical properties of the reactive TPNPs. The optical properties were characterized by the fluorescence emission spectrum of TPNPs. At the very beginning, WWW was used to prepare TPNPs1 to verify the importance of metal ion coordination and the importance of heating. In addition to designing and manufacturing peptide nanoparticles according to the normal process, a control experiment without heating and Zn(II) was also established. According to the results, under the excitation light of 370 nm, the fluorescence emission peak of TPNPs1 is about 515 nm (Fig. 1a), which is a green light in the visible light range. Compared with no Zn(II) coordination, Trp-Trp-Trp monomer, and reaction at room temperature (RT), the TPNPs obtained with Zn(II) coordination and heating have an obvious higher fluorescence intensity and the fluorescence peak is around 515 nm. In comparison, almost no fluorescence was produced in other groups. These results demonstrated that the reaction system of Zn(II) coordination and heating is necessary for the self-assembly of TPNPs1. In the process of self-assembly, Zn(II) and tripeptide are energy-favorable for assembly by initiating the interaction between ions and peptides. So, Zn(II) is pulled from the environment to a low peptide-rich in the dielectric environment, and form a more highly complex ordered structure which promoting the self-assembly of the tripeptide. The quantum confinement phenomenon may occur result from the self-assembled building blocks of Zn(II) and WWW tripeptide in sub-nano-scale coordination. The quantum confinement phenomenon may also lead to the red shift of TPNPs1 and the fluorescence of visible light region.

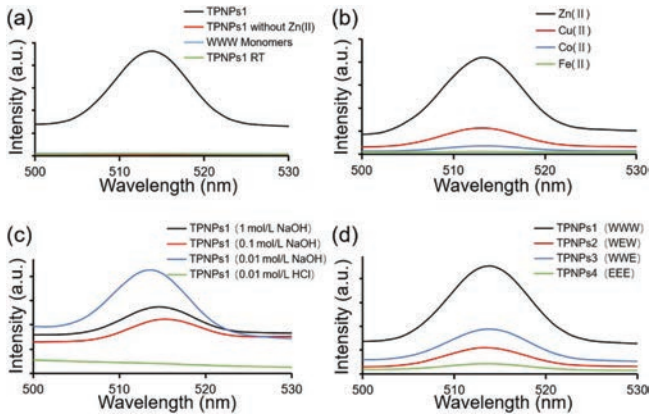

Fig. 1. Optical characterization of TPNPs. (a) Fluorescence emission spectra of WWW self-assembly with Zn(II) coordination, WWW self-assembly without Zn(II) coordination, WWW monomer, WWW self-assembly with Zn(II) coordination at room temperature (RT). (b) Fluorescence emission spectra of WWW self-assembly (TPNPs1) with the coordination of Zn(II), Cu(II), Co(II), and Fe(II), respectively. (c) Fluorescence emission spectra of WWW self-assembly (TPNPs1) with 1, 0.1, 0.01 mol/L NaOH and 0.01 mol/L HCl, respectively. (d) Fluorescence emission spectra of WWW self-assembly (TPNPs1), WEW self-assembly (TPNPs2), WWE self-assembly (TPNPs3), EEE self-assembly (TPNPs4).

Moreover, the reaction system becomes more active because of the heating, which speeds up the rate of movement of the molecules, provides the energy for self-assembly, and speeds up the self-assembly. In addition to Zn(II) coordination, various metal ions (Co(II), Cu(II), Fe(II)) were also applied to the self-assembly conditions of tripeptide nanoparticles. It can be seen that the fluorescence emission of the tripeptide coordinated by Co(II), Cu(II), and Fe(II) (Fig. 1b) is not significantly enhanced, while the fluorescence enhancement of Zn(II) is the largest. The transition metal ion Zn(II) could form a rigid chelate structure with the peptide due to the highest polarizability of Zn(II) among these metal ions while limiting further energy dissipation during thermal relaxation and obtaining stronger fluorescence. Later, the relationship between pH values and the fluorescence intensity of self-assembled TPNPs1 was explored by controlling the concentration of NaOH utilized in the experiment. It was found that the fluorescence intensity of TPNPs1 was the highest when the NaOH concentration was 0.01 mol/L. When the reaction environment became weak acidic, almost no fluorescence was generated. These results indicate that the weakly acidic environment is not suitable for WWW self-assembly, and the weakly alkaline environment is more favorable for self-assembly (Fig. 1c). Besides, in order to imitate the complex ionic environment in the organism, PBS was selected as the solvent to re-dissolve the initially obtained TPNPs1 precipitate. In addition, to understand whether it is the ionic environment or the pH has a great influence on the fluorescence intensity, water with a pH of 7.4 and pure water were selected (Fig. S5 in Supporting information). The TPNPs1 in PBS had the lowest fluorescence intensity, while the fluorescence intensity of TPNPs1 in deionized water and pH 7.4 water solution was similar. It is speculated that the complexion system in PBS may affect the fluorescence intensity. Therefore, the optimal condition for the self-assembly of the WWW tripeptide is at a mixed solution of MeOH and 0.01 mol/L NaOH by heating with Zn(II) coordination at 85 °C.

Finally, four types of TPNPs were prepared under similar conditions determined in the previous experiment. The tripeptide nanoparticles self-assembled from WWW, WEW, WWE, and EEE are TPNPs1, TPNPs2, TPNPs3, TPNPs4, respectively. In terms of the results, it can be found that different types of TPNPs all have a fluorescence peak at 515 nm, which is green fluorescence in the visible light range (Fig. 1d). TPNPs1 with the most aromatic amino acid residues has the highest fluorescence intensity, while TPNPs4 with amino acid residue side chains that do not contain a benzene ring has the lowest fluorescence intensity. The fluorescence intensities of TPNPs2 and TPNPs3 with moderate aromatic amino acids are in between. It is proved that in the process of self-assembly of TPNPs, in addition to the delocalization of electrons caused by hydrogen bonding so that low-energy electrons can be utilized by Zn(II) coordination, π-π stacking interaction also plays a considerable role. The benzene ring can serve as a driving force for self-assembly and increase the polarizability of electrons, which also enhances the fluorescence of TPNPs.

To understand the morphological characteristics of TPNPs more intuitively and determine their potential as drug carriers or fluorescent probes, four types of TPNPs were observed by atomic force microscopy (AFM), and the potential crystal structures of TPNPs1 were obtained by transmission electron microscopy (TEM). To better observe the morphology of peptide nanoparticles, a dilution operation was applied to the obtained TPNPs solution to prevent the accumulation of peptide nanoparticles. As shown in the AFM image, TPNPs1 are spherical particles with a relatively uniform size (Fig. 2c). From the TEM images, it can be seen that the diameter of TPNPs1 is about 5 nm (Figs. 2a and b). This is also consistent with the sub-nano-scale coordination of Zn(II) and tripeptide previously speculated. Compared with previous self-assembled peptide nanoparticles, this diameter is already small enough, which means that TPNPs1 can enter the cell more easily, and has the potential to be used as a drug carrier or fluorescent probe. TPNPs2 are irregular particles, and the diameter is much larger than TPNPs1 (Fig. 2d). Regardless of the degree of uniformity, the particle size or fluorescence intensity is also not as good as TPNPs1. The larger particles make it more difficult for TPNPs2 to enter the cell, which is not an ideal choice for nano-drug carriers. TPNPs3 even showed random fibrous self-assembly (Fig. 2e), which made it hard to be used for nanomedicine. The average diameter of TPNPs4 (Fig. 2f) is about 10 nm, but the particle size is not standardized, and the fluorescence intensity is not superior to other TPNPs. Through TEM and AFM images, it can be found that TPNPs1 is not only stronger than other peptide nanoparticles in terms of particle uniformity but also has a large advantage in particle size.

Previously, it has been proposed to use natural nanoparticles for drug delivery and cell imaging, and researchers also used dipeptide nanoparticles similar to tripeptide nanoparticles for targeted cancer cell imaging and real-time monitoring of drug release [14]. Inspired by the above study, TPNPs were explored as a drug carrier for cell imaging and drug monitoring. The common anthracycline chemotherapy drug DOX was selected to conjugate with TPNPs. An equal amount of DOX solution was mixed with four types of TPNPs and incubated in a shaker at 37 °C for 12 h. After that, the mixed solution was taken out and centrifuged to obtain a precipitate of supernatant and TPNPs + DOX. The color of the supernatant obtained by centrifugation can clearly show the binding efficiency. The darker the color in the supernatant, the lower the binding efficiency of TPNPs and DOX. It can be seen that the binding efficiency of TPNPs1 and DOX is the highest, while the binding efficiency of TPNPs4 and DOX is the lowest (Fig. S6 in Supporting information). The level of binding efficiency can also be learned according to the color depth after re-dissolving the TPNPs + DOX precipitate (Fig. S7 in Supporting information). The fluorescence emission pattern obtained by the fluorescence intensity of the supernatant also could verify the results (Fig. 3a). It can be intuitively found that the results are consistent with the speculation. It has been known from previous reports that DOX and aromatic amino acid-containing peptide nanoparticles are combined by electrostatic interaction and π-π stacking interaction, but TPNPs4 do not contain aromatic residues, so it may be combined with DOX only by electrostatic interaction. According to DLS data (Figs. S8–S11 in Supporting information), TPNPs1 and TPNPs4 are negatively charged, which can be better conjugated with DOX due to their positive charge. Interestingly, TPNPs2 has almost no charge, and TPNPs3 has a weak positive charge, which means that the binding efficiency of TPNPs3 and TPNPs4 to DOX should be lower than TPNPs4. However, both TPNPs2 and TPNPs4 had a higher binding rate with DOX than TPNPs4. We speculate that the π-π stacking interaction between TPNPs and DOX is stronger

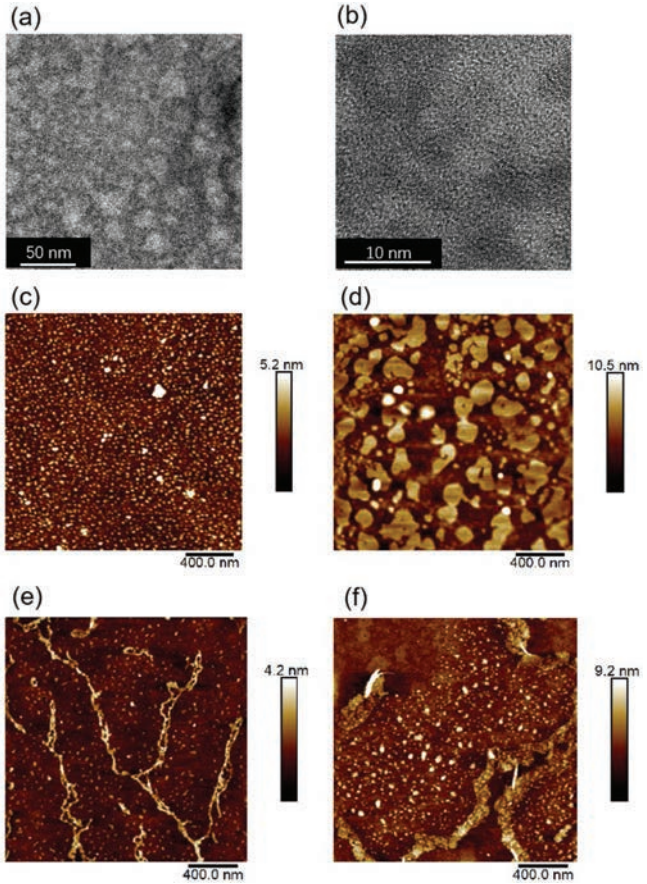

Fig. 2. Morphological characteristics of TPNPs. (a) The TEM images of TPNPs1 show uniform spherical nanoparticles. (b) The crystal structures of TPNPs1. (c) The AFM image of TPNPs1. (d) The AFM image of TPNPs2 shows uneven flat nanostructures. (e) The AFM image of TPNPs3 shows fibrous nanostructures. (f) The AFM image of TPNPs4 shows uneven spherical nanoparticles.

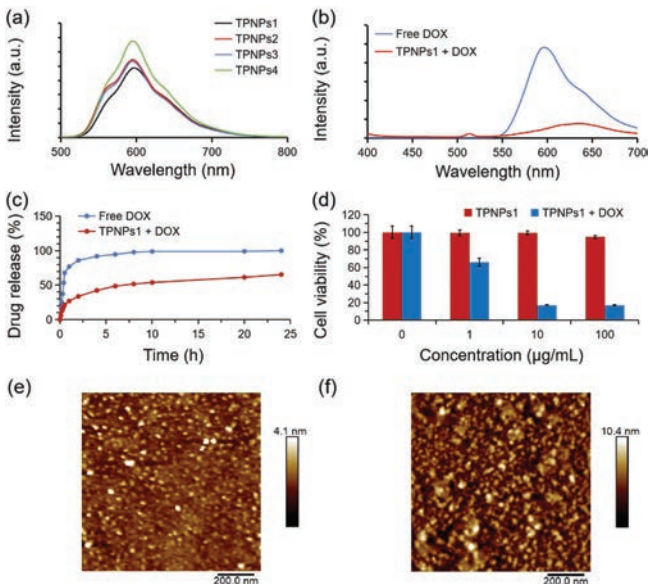

Fig. 3. Characteristics of TPNPs + DOX. (a) Fluorescence emission spectra of residual DOX in the supernatant after DOX conjugation with different TPNPs. (b) Fluorescence emission spectra of DOX before and after conjugation with TPNPs1 shows fluorescence quenching occurred at 595 nm. (c) Characterization of the release of DOX from the TPNPs1 + DOX conjugates. (d) Toxicity evaluation and comparison for the control, TPNPs1 + DOX, and free DOX against Hela cells. The AFM images of TPNPs1 (e) and TPNPs1 + DOX (f).

than the electrostatic effect. Therefore, when TPNPs2 and TPNPs3 conjugated to DOX, the effect of π-π stacking offsets the adverse effect caused by the charge, resulting in a higher binding rate than TPNPs4.

Through the above experiments, among the four nanoparticles, TPNPs1 not only has the highest fluorescence intensity, but also has the highest binding efficiency with DOX, which meets the requirements of the experiment to the greatest extent. So, the TPNPs1 was selected to further explore its biomedical applications. To determine whether TPNPs1 and DOX are indeed mutually conjugated, the fluorescence spectra were applied in the process. Compared with Free DOX, the fluorescence intensity of TPNPs1 + DOX at the same dox concentration decreased significantly due to the fluorescence quenching at 595 nm (Fig. 3b), which also proves the interaction between TPNPs1 and DOX. In this process, we found an interesting phenomenon: the light emission area of TPNPs1 overlaps with the excitation light area of DOX, which means there is a fluorescence resonance phenomenon between them. Therefore, it is proposed that the TPNPs1 could be used to monitor the release of DOX in real time from TPNPs1 + DOX. The AFM images of TPNPs1 + DOX (Fig. 3f) showed larger nanoparticles than TPNPs1 (Fig. 3e), which demonstrated the conjugation between TPNPs1 and DOX. To study the feasibility of TPNPs1 for drug delivery and release, we set equal amounts of free DOX and TPNPs1 + DOX into dialysis tubes respectively, and then put them into PBS solution for sustained release experiment. At regular intervals, a 1 mL PBS solution was taken to detect the fluorescence intensity of DOX, to determine the released amount of DOX in PBS. The release rate was calculated according to the absorption intensity and a trend graph was drawn (Fig. 3c). It can be seen that free DOX is released at 12 h, while TPNPs1 released 60% of DOX and still released slowly after 24 h. The results indicated that TPNPs1 can release most of the DOX into the environment and can be used for long-term treatment of lesions. The longer sustained release time allows the drug to maintain a high concentration for a long time, preventing the problem of the short half-life of the drug due to metabolism or other reasons. A longer half-life can reduce the frequency of drug use and improve the utilization rate of the drug during treatment. Afterward, to study the cytotoxicity of TPNPs1, a cytotoxicity test was conducted. The cell viability after incubating with Hela cells using TPNPs1 and TPNPs1 + DOX at four concentrations of 0, 1, 10, and 100 μg/mL, respectively. TPNPs1 still has very low cytotoxicity even at the highest concentrations, and TPNPs1 + DOX still retains its killing effect on cells even at lower concentrations (Fig. 3d). These results demonstrated that TPNPs1 can indeed be used as a peptide nanoparticle that is not harmful to health, while the DOX carried can remain its killing effect on cancer cells.

Cellular imaging of Hela cells incubated with TPNPs1 + DOX was recorded through confocal microscopy, which clearly showed the function of TPNPs1 + DOX in cell imaging and monitoring of drug release (Fig. 4). After 1 h incubation, only weak fluorescence was observed. With the extension of incubation time, more TPNPs1 + DOX entered the cell, and TPNPs1 also released more DOX. Therefore, the fluorescence signals of TPNPs1 and DOX are increasing. The fluorescence of TPNPs1 is highly coincident with the DOX fluorescence signal. According to Fig. 3b, it can be learned that there is fluorescence resonance between TPNPs1 and DOX. In Fig. 4, it can be clearly observed through fluorescence intuitively. When the excitation was 370 nm, TPNPs1 should emit green fluorescence (515 nm), and 480 nm excitation can excite free DOX to emit red fluorescence. When 370 nm excitation was used to irradiate the TPNPs1 + DOX, the red fluorescence (600 nm) emitted by DOX in the nanocomposite was also received. Therefore, there is an energy transfer between TPNPs1 and DOX, which is fluorescence resonance.

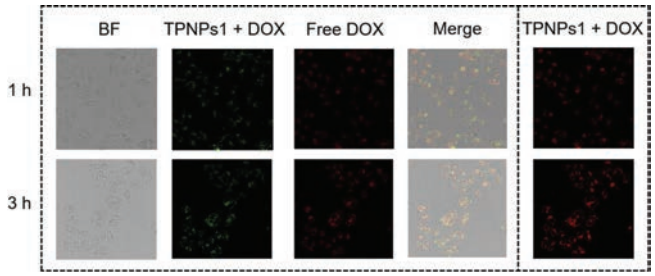

Fig. 4. Representative fluorescence images of Hela cells incubated with TPNP1 + DOX conjugates. After 1 h, only negligible fluorescence was discovered. After 3 h, relatively strong intensity of the TPNPs1 + DOX (right part, Ex: 370 nm, Em: 600 nm), TPNPs1 + DOX (left part, Ex: 370 nm, Em: 515 nm) and free DOX (Ex: 480 nm, Em: 600 nm) was seen, which can be attributed to more DOX releasing from the TPNPs1 + DOX conjugates and more TPNPs1 + DOX entering in the cells. Green, the fluorescence signal of the TPNPs1 and TPNPs1 + DOX; red, the fluorescence signal of DOX and TPNPs1 + DOX.

In summary, this study developed several new tripeptide nanoparticles based on zinc coordination and π-π stacking. According to the fluorescence intensity and the binding rate with DOX, TPNPs1 prepared by tripeptide containing only tryptophan residue was the best option for bio-imaging and drug delivery applications. These self-assembled tripeptide nanoparticles all can stimulate green visible fluorescence under ultraviolet light. Besides, *in vitro* cytotoxicity tests have confirmed that the nanoparticles have almost no toxic effect on cells, but the delivered DOX has a strong killing effect on cancer cells. In conclusion, the current work proves that tripeptide self-assembled nanoparticles can be used for cell imaging and real-time drug monitoring while delivering drugs, which also opens up a new avenue for design and prepare fluorescent nanoparticles for bioimaging and drug delivery applications.

Declaration of competing interest

The authors declare that they have no known competing financial interests or personal relationships that could have appeared to influence the work reported in this paper.

Acknowledgments

This work was supported by the National Natural Science Foundation of China (Nos. 31900984 and 31971315), the Natural Science Basic Research Plan in Shaanxi Province of China (No. 2019JQ-231), the China Postdoctoral Science Foundation (No. 2018M631197), the Shaanxi Postdoctoral Science Foundation (No. 2018BSHQYXMZZ42), the Fundamental Research Funds for the Central Universities (No. 31020180QD063). We would like to thank the Analytical & Testing Center of Northwestern Polytechnical University for the TEM and AFM characterization.

Appendix A. Supplementary data

Supplementary material related to this article can be found, in the online version, at doi:https://doi.org/10.1016/j.cclet.2020.07.011.

References

[1] S. Sun, Q. Guan, Y. Liu, et al., Chin. Chem. Lett. 30 (2019) 1051–1054.
[2] Z. Chen, C. Wu, Z. Zhang, et al., Chin. Chem. Lett. 29 (2018) 1601–1608.
[3] C.X. Yang, L. Xing, X. Chang, et al., Mol. Pharm. 17 (2020) 1300–1309.
[4] P. Zheng, Y. Liu, J. Chen, et al., Chin. Chem. Lett. 31 (2020) 1178–1182.
[5] L. Sun, A. Li, Y. Hu, et al., Part. Part. Syst. Charact. 36 (2019)1800420.
[6] M. Sun, H. Hu, L. Sun, Z. Fan, Chin. Chem. Lett. 31 (2020) 1729–1736.
[7] L. Sun, Y. Hu, L. Zhang, Curr. Pharm. Des. 24 (2018) 2394–2402.

[8] W. Gao, Y. Hu, L. Xu, et al., Chin. Chem. Lett. 29 (2018) 1795–1798.
[9] L. Sun, Z. Fan, T. Yue, et al., Bio-Des. Manuf. 1 (2018) 182–194.
[10] T. Fan, X. Yu, B. Shen, L. Sun, J. Nanomater. 2017 (2017) 4562474.
[11] L. Sun, Z. Fan, Y. Wang, et al., Soft Matter 11 (2015) 3822–3832.
[12] Y. Sun, A. Zhan, S. Zhou, et al., Chin. Chem. Lett. 30 (2019) 1435–1439.
[13] K. Tao, Z. Fan, L. Sun, et al., Nat. Commun. 9 (2018) 3217.
[14] Z. Fan, L. Sun, Y. Huang, Y. Wang, M. Zhang, Nat. Nanotechnol. 11 (2016) 388–394.
[15] Z. Fan, Y. Chang, C. Cui, et al., Nat. Commun. 9 (2018) 2605.
[16] G.B. Qi, Y.J. Gao, L. Wang, H. Wang, Adv. Mater. 30 (2018) 1703444.
[17] W. Ma, S.N. Sha, P.L. Chen, et al., Adv. Healthc. Mater. 9 (2020) 1901100.
[18] T. Guo, L. Wang, S. Sun, et al., Chin. Chem. Lett. 30 (2019) 1253–1260.
[19] Y. Xu, M. Tian, H. Zhang, et al., Chin. Chem. Lett. 29 (2018) 1093–1097.
[20] M. Yu, D. Su, Y. Yang, et al., ACS Appl. Mater. Interfaces 11 (2019) 176–186.
[21] X. Shi, P. Yang, X. Peng, et al., Polymer 170 (2019) 65–75.
[22] S. Yun, H. Lee, W.E. Lee, H.S. Park, Fuel 174 (2016) 36–42.
[23] H. Yu, T. Man, W. Ji, et al., Chin. Chem. Lett. 30 (2019) 175–178.
[24] C. Chen, X. Ji, Chin. Chem. Lett. 29 (2018) 1287–1290.
[25] J. Kong, J. Zhang, Y. Wang, et al., ACS Appl. Mater. Interfaces 12 (2020) 4212–4220.